18 September 2026

Estimating Tsunami Currents in a Resonant Harbor Using Video-Based Analysis: Application to Crescent City, California

Gregory B. Crawford[1], Giulio Dolcetti[2], Amanda R. Admire[3], Burak Uslu[4]

1. Faculty of Science, Ontario Tech University
2. Dept. Environmental Sciences, Informatics and Statistics, Foscari University of Venice
3. Dept. Geology and Dept. Oceanography, California State Polytechnic University
4. OMC International

Abstract

Crescent City Harbor, California, is well known for experiencing severe tsunami impacts. While NOAA tide gauges have routinely measured tsunami water levels for decades, direct observations of tsunami currents in the region remain scarce. Here, we analyze 12 hours of continuous security camera video using wave-dispersion-corrected optical velocimetry (Image Wave Velocimetry) to derive high-resolution surface velocity fields near the small boat basin entrance during the 2025 Kamchatka tsunami. This represents the first application of this technique to continuous tsunami current observations. We demonstrate that moderate vertical water-level fluctuations (±1.1 m) sustained strong surface currents (up to 2.6 m s-1) over dozens of resonant cycles for hours following the initial arrival. Horizontal velocity and surface displacement were in quadrature, consistent with classical theory for standing waves in a semi-enclosed basin. The analysis also resolves the formation and evolution of coherent eddies at the basin entrance.

Estimating Tsunami Currents in a Resonant Harbor Using Video-Based Analysis: Application to Crescent City, California

Gregory B. Crawford[1],*, Giulio Dolcetti[2], Amanda R. Admire[3], and Burak Uslu[4]

[1] Faculty of Science, Ontario Tech University, Oshawa, Ontario, Canada

[2] Dept. Environmental Sciences, Informatics and Statistics, Ca' Foscari University of Venice, Venice, Italy

[3] Dept. Geology and Dept. Oceanography, California State Polytechnic University, Humboldt, Arcata, CA, USA

[4]OMC International, Abbotsford, Victoria, Australia

* Corresponding author: Gregory Crawford (greg.crawford@ontariotechu.ca)

ORCID IDs:

Gregory B. Crawford: https://orcid.org/0000-0003-3194-4576

Giulio Dolcetti: https://orcid.org/0000-0002-0992-0319

Amanda R. Admire: https://orcid.org/0009-0005-6125-9635

Burak Uslu: https://orcid.org/0000-0003-2122-0152

Key Points:

- A security camera at Crescent City Harbor captured the 2025 Kamchatka tsunami during daylight hours.
- Wave-corrected optical velocimetry derived surface velocity fields at 1-minute resolution.
- The observed phase lag between tsunami sea level and velocity at the boat basin entrance matches standing wave theory for a semi-enclosed basin.

Abstract

Crescent City Harbor, California, is well known for experiencing severe tsunami impacts. While NOAA tide gauges have routinely measured tsunami water levels for decades, direct observations of tsunami currents in the region remain scarce. Here, we analyze 12 hours of continuous security camera video using wave-dispersion-corrected optical velocimetry (Image Wave Velocimetry) to derive high-resolution surface velocity fields near the small boat basin entrance during the 2025 Kamchatka tsunami. This represents the first application of this technique to continuous tsunami current observations. We demonstrate that moderate vertical water-level fluctuations (±1.1 m) sustained strong surface currents (up to 2.6 m s^{-1}) over dozens of resonant cycles for hours following the initial arrival. Horizontal velocity and surface displacement were in quadrature, consistent with classical theory for standing waves in a semi-enclosed basin. The analysis also resolves the formation and evolution of coherent eddies at the basin entrance.

Introduction

Tsunami-driven currents can cause catastrophic damage within ports and harbors, often inflicting severe infrastructure losses thousands of kilometers from the earthquake epicenter (e.g., Borrero et al., 2015). During the 2011 Tohoku-oki tsunami, while direct overland inundation along the California coast was minimal due to the tsunami arriving during low tide, powerful horizontal currents damaged over two dozen maritime facilities, resulting in more than $50 million USD in financial losses (Wilson et al., 2012). Such events underscore that hazardous horizontal flows can persist independently of severe vertical flooding, prompting widespread recommendations to incorporate current velocity predictions into operational tsunami warning products (e.g., Lynett et al., 2014; Bernard and Titov, 2015).

Despite the recognized hazard, direct observations of tsunami currents remain extremely rare compared to water-level observations. While coastal tide gauges have routinely recorded real-time sea surface elevations at high temporal resolution (e.g., 1-minute intervals) for decades, direct current measurements are far less prevalent. In the United States, real-time current profilers are primarily restricted to high-traffic commercial ports through NOAA's Physical Oceanographic Real-Time System (PORTS)—such as San Francisco Bay, Humboldt Bay, and Anchorage—due to high installation and maintenance costs. In other locations, current observations are limited to short-term research deployments. In Crescent City, California (Fig. 1a)—a site well-known for severe tsunami amplification—an acoustic Doppler current profiler (ADCP) was mounted at Citizens Dock in 2013 adjacent to the NOAA tide gauge (Fig. 1b). Although this instrument recorded currents during a small tsunami in 2014 (Crawford et al., 2017), it was subsequently removed in 2015, leaving the harbor once again without continuous current instrumentation.

To bridge this observational gap, video-based remote sensing has emerged as a powerful tool for estimating tsunami current velocities. Fritz et al. (2006, 2012) pioneered the use of survivor videos combined with post-event 3D LiDAR/GPS calibration and Large-Scale Particle Image Velocimetry (LSPIV) to reconstruct overland flow speeds during violent, short-duration tsunami inundations. In far-field harbor settings, Admire et al. (2014) and Kalligeris et al. (2016) demonstrated that Lagrangian tracking of floating debris could yield quantitative current estimates in constricted channels. However, these earlier far-field approaches suffered from notable observational constraints. Admire et al. (2014) relied on a 3.5-hour security camera segment from the 2011 Tohoku event in Crescent City—a record cut short by power shutoffs—and required labor-intensive manual tracking of individual debris particles on-screen (Admire, 2013). More fundamentally, standard particle tracking and optical velocimetry methods do not account for ambient wind-waves and swell, which can cause surface brightness patterns to propagate at wave phase speeds rather than true fluid velocity.

Here, we overcome these limitations by presenting a continuous 12-hour video analysis of tsunami-driven currents near the entrance of the small boat basin in Crescent City, recorded by a fixed security camera during the July 2025 Kamchatka tsunami. To our knowledge, this represents the first application of wave-dispersion-corrected optical velocimetry—which explicitly accounts for the ambient surface wave spectrum—to continuous tsunami current observations. This automated, physics-based approach decouples phase propagation from mean fluid advection, yielding high-resolution spatiotemporal surface velocity fields without requiring physical tracer objects. With this unprecedented 12-hour record, we capture the temporal evolution of tsunami currents, documenting how moderate water-level fluctuations (±1.1 m) drive sustained, high-velocity currents (up to 2.6 m s^{-1}) and localized vortex shedding across dozens of resonant cycles hours after the initial arrival.

Materials and methods

1. Water Level Observations and Processing

Continuous 1-minute preliminary water level observations at Crescent City, CA (Station ID: 9414806) were retrieved from the NOAA Center for Operational Oceanographic Products and Services (CO-OPS) Data Retrieval API (NOAA CO-OPS, 2025). The tide gauge is located at Citizen's Dock in Crescent City Harbor (Fig. 1b). Water level elevations were evaluated relative to Mean Lower Low Water (MLLW) and referenced to Pacific Daylight Time (PDT; UTC-7) for temporal consistency with the video footage. The 1-minute timestamps correspond to the midpoint of each averaging interval. To isolate the tsunami signal, the water level time series was detided by applying an 8th-order net phase-preserving (zero-phase) high-pass Butterworth filter with a 3-hour cutoff period.

2. Video Acquisition and Ortho-Rectification

Continuous video footage of Crescent City Harbor was acquired using a Ubiquiti UniFi G4 Pro (UVC-G4-Pro) security camera mounted on the roof of the Crescent City Harbor District Office, oriented approximately west toward the Battery Point Lighthouse. The camera recorded at a resolution of 3840 × 2160 pixels, 24 frames per second (fps), and 16 bits per pixel. The recorded footage was temporarily archived on a secure server with near-real-time timestamps assigned upon capture. Video files spanning July 29 through August 3, 2025, were provided by the Harbor District; daylight observations from July 30 (06:10 to 19:13 PDT) were analyzed in this study.

Video frames were ortho-rectified and reprojected onto a horizontal plane corresponding to the instantaneous water surface using the open-source Python package *pyopenrivercam*. Ortho-rectification was performed by establishing nine distinct ground control points (GCPs) in the initial frame and linking them to geographical coordinates extracted from high-resolution satellite imagery (Google Earth). To account for tide and tsunami stage changes, the vertical elevation of the reprojection plane was dynamically adjusted in time according to the reconstructed water surface level time series. The resulting ortho-rectified frames had a spatial resolution (pixel size) of 0.2 m and covered a total area of approximately 160 m × 160 m.

3. Wave-Dispersion-Corrected Optical Velocimetry (IWaVE)

Spatiotemporal surface velocity vector distributions were derived using the open-source image velocimetry software IWaVE (Dolcetti et al., 2022, Winsemius et al., 2026). Surface velocity estimates are extracted by fitting the observed space-time Fourier spectrum of the video sequence to a theoretical multivariate Doppler-shifted dispersion relation. The observed surface patterns are assumed to follow either the linearized water wave dispersion relation in deep water:

$$\omega = \sqrt{g|k|} + k \cdot U$$

or a simplified “rigid-advection” relation:

$$\omega = k \cdot U$$

where ω is the angular frequency, **k** is the wavevector, g is gravitational acceleration, and **U** is the surface velocity vector. The deep-water relation accounts for the space-time spectral signature of free-surface gravity waves, whereas the rigid-advection relation captures passive surface tracers such as flotsam, foam, or turbulent boils advected by the background mean flow (e.g., Muraro et al., 2021). IWaVE employs a genetic algorithm to optimize the fit between these two theoretical relations and the 3D Fourier spectrum of the video. While finite water depth and vertical velocity shear can be incorporated into the dispersion model, they were neglected here as they were difficult to quantify uniformly over the entire domain.

The velocimetry algorithm was applied to contiguous 60-second ortho-rectified video clips. Each clip was spatially partitioned into non-overlapping 50 × 50 pixel^2 (10 m × 10 m) interrogation windows. Fourier spectra for each window were computed by averaging over 10-second sub-clips with 50% overlap to smooth spectral noise and ensure optimization convergence. Each spatial window and 60-second clip were processed independently, yielding a dense grid of quasi-local velocity vector estimates with a spatial resolution of 10 m and a temporal sampling frequency of 1/60 Hz. Default IWaVE settings were used, except the genetic algorithm population size was increased to 16 to ensure convergence to the global optimum.

4. Quality Control, Outlier Filtering, and Point Extraction

The accuracy of image velocimetry measurements using spectral dispersion fitting relies on several fundamental optical and physical assumptions (Dolcetti et al., 2022). Surface waves and deformations must be visually detectable by the camera, and their space-time spectra must adhere to the theoretical dispersion relations derived from linearized wave theory. In the harbor environment, surface waves are primarily rendered visible as modulations in reflected sky intensity caused by local surface slope variations, which depend directly on light reflectance angles and the azimuthal distribution of sky color. Under challenging visibility or lighting conditions, the resulting 3D Fourier spectra become significantly noisier. Furthermore, non-linear wave dynamics and steep free-surface deformations introduce harmonics and spectral leakage that deviate from linear dispersion theory.

To evaluate spectral fidelity, IWaVE computes an empirical quality metric ($Q \in [0,1]$) quantifying the goodness-of-fit between the observed Fourier spectrum and the theoretical dispersion relation ($Q = 1$ representing an ideal match). To ensure high confidence in the velocity field, all estimates with $Q < 0.8$ were discarded. Residual spatial and temporal outliers were subsequently identified and removed using an iterative median filter without replacement.

In addition to environmental noise, localized obstructions can violate the passive-tracer and wave-dispersion assumptions. Boats moving through the harbor entrance disrupted the water surface, creating non-physical velocity anomalies. A total of 68 one-minute video clips containing boat traffic were visually identified and removed from the analysis. Following quality filtering and clip exclusion, the final continuous velocity time series spanned from 06:10 to 19:13 PDT on July 30.

Local velocity time series were extracted at specific points of interest across the 160 m × 160 m domain by applying a quality-weighted spatial interpolation of valid vectors within a 30 m × 30 m bounding box. Primary analysis focuses on the entrance to the small boat basin (Fig. 1b), corresponding to the location where Admire et al. (2014) estimated currents manually from 3.5 h of video for the 2011 Tohoku tsunami.

To complement the tide gauge observations, a local secondary water-level time series was derived directly from the video feed by tracking the vertical motion of a floating dock near the harbor entrance. As the dock rose and fell, it exposed a varying length of its support piling, which exhibited a dark visual contrast relative to the surrounding structures. The lower visible edge of the piling was detected in each frame by identifying the vertical pixel coordinate at which a specified greyscale intensity threshold was crossed. Pixel height was converted to physical vertical displacement using a calibration measurement taken on May 29, 2026, at ~07:00 PDT near low tide (-0.15 m MLLW at 05:31 PDT), when the distance from the top of the piling to the dock interface was physically measured at 4.61 m. To reduce high-frequency surface chop and camera vibration noise, and to align with the

NOAA 1 min observations, vertical tracking was performed on 1-minute running-average images across the study period.

Cross-spectral, coherence, phase, and cross-correlation analyses between water level and current were performed following standard digital signal processing techniques (e.g., Bendat & Piersol, 2011). Spectral estimates used Welch-style averaging with a Hamming window and dataset-specific segment lengths. Phase values were only plotted when the associated coherence was above a threshold ($C^2 \geq 0.5$; e.g., Elipot et al., 2013). Custom MATLAB scripts were developed for data analysis using MATLAB Copilot (The Mathworks, Inc., release R2026a) as an assistive coding tool. All generated algorithms were independently tested, debugged, and validated prior to final data processing.

To contextualize the observed harbor dynamics and compare against past events, numerical tsunami simulations were performed using NOAA's Method of Splitting Tsunamis (MOST) suite (Titov & González, 1997; Titov & Synolakis, 1998). MOST solves the non-linear shallow-water equations over a nested-grid system that reaches a fine-scale spatial resolution of 1 arc-second (~30 m) within Crescent City Harbor. We re-examine model output for the 11 March 2011 Tohoku event (Admire et al., 2014) alongside new simulations for the 29 July 2025 Kamchatka event. Modeled elevation and horizontal velocity time series were extracted at the small boat basin entrance and rotated to align with the primary channel axis. Full details regarding nested grid hierarchies, bathymetry, and seismic source formulations are provided in Text S1.

Results

The July 30, 2025 Kamchatka tsunami arrived at Crescent City Harbor at approximately 00:24 PDT. Detided sea surface elevation records from the NOAA tide gauge at Citizens Dock (Fig. 2a) indicate a maximum tsunami amplitude of 1.10 m at 01:45 PDT. By 19:00 PDT, peak wave amplitudes decayed to approximately half this value (~0.55 m), with persistent resonant ringing continuing across the subsequent three days.

Sea surface elevation extracted optically from the floating dock closely matches the detided NOAA gauge record for the overlapping observation period (06:10–19:13 PDT; Fig. 2b). Discrepancies between the two instruments are minor, occurring predominantly prior to 07:00 PDT. Cross-correlation indicates the floating dock water level lagged the Citizens Dock gauge by approximately 2 min (not shown).

An example of the derived flow field is shown in Fig. 1d, corresponding to a 1-minute average starting at 09:08 PDT, near the peak of a tsunami “flood” phase. Velocities are strong from the entrance into the boat basin (as far as the camera field of view extends), peaking at approximately 3.39 m s^{-1} deep into the basin. Currents in the outer harbor are weaker; velocity vectors indicate clear spatial convergence as flow funnels through the entrance into the basin. A video showing the retrieved flow fields throughout the entire observation period is provided in Movie S1.

The observed flow at the basin entrance and within the channel was predominantly one-dimensional along the primary channel axis (Fig. S1a). Figure 2c presents the extracted velocity time series at the entrance (Fig. 1a) oriented along this dominant flow direction following detiding. The peak flood current reached or exceeded 2.0 m s^{-1} five times between 06:10 and 09:13 PDT, after which current speeds generally decayed.

Figure 3a depicts the velocity field at 06:19 PDT during the formation of a transient eddy at the basin entrance, with streamlines overlaid to highlight the recirculating structure. A corresponding video frame (06:19:37 PDT) visually confirms the feature in the raw footage. [The eddy spanned approximately 50 m in diameter, with outer rim speeds on the order of 1 m s^{-1} and localized vertical vorticity peaking at roughly 0.1 s^{-1}.] The eddy formed as strong shear flow detached past the end of the breakwater, just west of the entrance.

Figure 4 describes the relationship between water level at the floating dock and current velocity at the basin entrance across multiple spectral metrics. The cross-power spectrum (Fig. 4a) exhibits a narrow spectral peak centered near 4.7×10^{-2} cpm (21 min period), with half-power (–3 dB) bounds at 0.044 cpm (22 min) and 0.049 cpm (20 min). Spectral coherence (Fig. 4b) is high across a broad range of tsunami frequencies. Phase (Fig. 4c) remains stable across the energetic frequency band (0.023–0.086 cpm; 12–43 min), ranging between –79° and –93° (averaging –86°). At the dominant 21-min peak frequency, this –86° phase lag corresponds to a current velocity lag of +5.1 min relative to water level elevation. Cross-correlation analysis (Fig. 4d) independently confirms a peak correlation at a lag of +5 min, with a zero-lag correlation coefficient of 0.13.

Figure 4 also includes corresponding observations from the 2011 Tohoku tsunami (dashed lines), adapted from Admire et al. (2014). This 3.5 h record—limited by the video duration available in 2011—shows an elevated cross-spectral energy density reflecting the larger magnitude of the 2011 event (Fig. 4a), with a broader, flatter spectral peak from 0.047 to 0.070 cpm (14–21 min). Coherence is similarly high across the tsunami band (Fig. 4b). However, phase values for the 2011 event were smaller, ranging from –42° to +3° between 0.01 and 0.1 cpm (–14° at 0.047 cpm, corresponding to a +1 min lag; Fig. 4c). Peak cross-correlation similarly occurs at a +1 min lag (Fig. 4d).

Time series of numerical model runs (MOST) for water level and currents at the basin entrance during the 2011 event were previously presented in Admire et al. (2014); equivalent model results for the 2025 event are shown in Fig. S2. Modeled entrance currents were also highly uni-directional (Fig. S1b) and were rotated to align with the primary channel axis. Cross-spectral analysis of the 2025 model output (Fig. S3) yields a phase shift of –66° at 0.047 cpm (21 min; noted in Fig. 4c) and a normalized cross-correlation peak at a lag of +3.5 min (Fig. 4d).

Discussion

Spectral phase and cross-correlation analyses confirm that the Crescent City small boat basin responds to far-field tsunami forcing as a semi-enclosed standing-wave resonator (e.g., Wilson, 1972; see Rabinovich, 2009 for review). Across the primary 12–43 min tsunami frequency band, observed horizontal currents and surface displacements exhibit an average phase difference of –86° (near-exact 90° quadrature). At the dominant 21 min resonant peak (0.047 cpm), velocity leads water elevation by 5.1 min — essentially ¼ of that period. This quadrature relationship reflects classical mass conservation in a constricted basin: maximum volume flux through the small basin entrance region drives the highest rate of water level change ($d\eta/dt$), while peak high and low water stages coincide with slack flow.

Numerical tsunami simulations using the Method of Splitting Tsunamis (MOST) for both the 2011 Tohoku and 2025 Kamchatka events capture similar elevation and velocity variability at the basin entrance, with a dominant resonant period near 21 min (Text S1, Figs. S1–S2). Spectral analysis of the modeled time series yields a slightly lower phase lag, remaining fairly flat around –67° across a broad frequency band with a cross-correlation peak at +4 min. Crucially, both observations and MOST model predictions remain firmly anchored near quadrature (–90°), characteristic of semi-enclosed basin standing waves, rather than in-phase behavior (0°) typical of progressive waves (e.g., Lamb, 1932; Dean & Dalrymple, 1991).

This resonant standing-wave response at Crescent City contrasts sharply with tsunami dynamics observed in nearby coastal estuaries. For example, in Humboldt Bay—located approximately 100 km south of Crescent City—tsunami surface displacements and channel velocity fields display phase lags much closer to 0°, reflecting a strongly damped progressive wave governed by extensive intertidal mudflats and bottom friction (Crawford et al., 2026). Together, these contrasting behaviors demonstrate how local estuarine geometry and frictional dissipation dictate whether far-field tsunami energy manifests as standing-wave resonance or damped progressive propagation along the northern California coast.

Direct comparison with the 2011 Tohoku tsunami observations at the same location (Admire et al., 2014) highlights how local flow speeds scale with forcing amplitude. During the initial 3 hours of the 2011 event, sea surface elevation fluctuations reaching ~2.5 m drove peak horizontal currents approaching 5.0 m s^{-1} at the small boat basin entrance. In contrast, our continuous video record for the 2025 Kamchatka tsunami captures the flow field beginning ~6 hours after initial arrival, during which water level fluctuations reached ±1.1 m and produced peak surface currents of 2.0 to 2.6 m s^{-1}. Despite differences in event magnitude and observational timing, the ratio of peak horizontal current speed to vertical water-level elevation remains remarkably consistent between the two events (e.g., ~2.0 to 2.3 s^{-1}).

The 12-hour optical dataset also captures transient localized features, such as the formation of a coherent eddy at the basin entrance at 06:19 PDT (Fig. 3c). In this instance, a strong shear flow developed past the end of the breakwater, just west of the entrance, during a period of relatively slack flow within the entrance channel itself, causing the shear layer to roll up into a distinct vortex. While fixed single-point observations cannot easily distinguish transient eddies from background flow variability, 2D optical surface mapping explicitly resolves their spatial structure and evolution. Such observations provide valuable real-world benchmarks for numerical models capable of resolving fine-scale shear dynamics and localized flow separation (e.g., Kalligeris et al., 2016), which contribute to non-linear energy dissipation in semi-enclosed harbors.

Evaluating precise phase relationships in basins with short dominant periods, such as Crescent City's 21-min resonance, requires strict temporal synchronization, as a 2-min timing offset corresponds to a ~35° phase shift. We attribute the minor phase disparity between the 2011 Tohoku observations (~2 min lag; Admire et al., 2014) and the present 2025 analysis (~5 min lag) primarily to unquantified clock drift in legacy video recording hardware, as well as the truncated 3.5-hour duration of the 2011 record. In contrast, deriving both horizontal surface currents (via IWaVE) and vertical surface elevations (via floating dock tracking) simultaneously from a single, continuous 12-hour video stream completely eliminates inter-instrument timing skew.

Ultimately, these results establish that security cameras, combined with wave dispersion-corrected video velocimetry analysis, represent a robust, low-cost approach for long-duration tsunami current and water level monitoring in vulnerable ports worldwide (at least during daylight hours), providing operational benchmarks for harbor hazard mitigation without specialized underwater instrumentation.

Acknowledgements

We would like to thank Mike Rademaker (Crescent City Harbormaster), Justin Hanks (Crescent City Harbor Patrol Dockmaster), and the Crescent City Harbor Maintenance and IT departments for providing the security camera footage and for collecting the on-site measurements used for georeferencing in this study. We also thank the NOAA Center for Operational Oceanographic Products and Services (CO-OPS) for maintaining the National Water Level Observation Network (NWLON) and providing high-frequency (1-minute) water level data, which remain essential for coastal hazard monitoring, tsunami research, and community resilience. GC acknowledges Ontario Tech University for providing administrative leave, during which much of the analysis and manuscript preparation for this study was conducted. GD acknowledges support within the framework of the DoE 2023–2027 (MUR, project AIS.DIP.ECCELLENZA2023_27.FF). The remaining authors received no external funding for this research.

Author Contributions

Gregory Crawford: Conceptualization, Methodology (Software and AI-Assisted Code Validation), Data Analysis, Visualization, Writing – original draft.

Giulio Dolcetti: Methodology, Software, Formal Analysis. Writing – review & editing.

Amanda Admire: Data Curation, Writing – review & editing.

Burak Uslu: Methodology, Software, Investigation, Writing – review & editing.

Open Research

Water level observations at 1-minute intervals were obtained from the NOAA CO-OPS Data Retrieval API web interface (https://api.tidesandcurrents.noaa.gov/api/prod/) for Station 9414806 (Crescent City, CA). The continuous time series analyzed in this study was compiled by stitching together consecutive 5-day data requests covering July 27 to August 10, 2025. A representative API request URL used to retrieve a portion of this dataset is:

https://api.tidesandcurrents.noaa.gov/api/prod/datagetter?begin_date=YYYYMMDD&end_date=YYYYMMDD&station=9414806&product=one_minute_water_level&datum=MLLW&time_zone=gmt&units=metric&format=csv

The open-source optical velocimetry software *IWaVE* is available via GitHub (https://github.com/DataForWater/IWaVE) and archived on Zenodo (Winsemius et al., 2026). Frame ortho-rectification was performed using *pyopenrivercam* (https://localdevices.github.io/pyorc/). All derived dataset files—including the 1-minute surface velocity vector fields, floating dock water level time series, and MOST numerical model outputs—are publicly archived on Zenodo (https://doi.org/10.5281/zenodo.22131854).

Due to privacy and institutional research ethics constraints regarding identifiable individuals, vehicles, and private vessels in public spaces, the raw, unedited security camera video footage is restricted. Processed or masked video segments used for velocimetry validation may be requested from the corresponding author for non-commercial academic research purposes.

References:

Admire, A. R., Dengler, L. A., Crawford, G. B., Uslu, B. U., Borrero, J. C., Greer, S. D., & Wilson, R. I. (2014). Observed and modeled currents from the Tohoku-oki, Japan and other recent tsunamis in northern California. *Pure and Applied Geophysics*, *171*(12), 3385–3403. https://doi.org/10.1007/s00024-014-0797-8

Bernard, E., & Titov, V. (2015). Evolution of tsunami warning systems and products. *Philosophical Transactions of the Royal Society A: Mathematical, Physical and Engineering Sciences*, *373*(2053), 20140371. https://doi.org/10.1098/rsta.2014.0371

Borrero, J. C., Lynett, P. J., & Kalligeris, N. (2015). Tsunami currents in ports. *Philosophical Transactions of the Royal Society A: Mathematical, Physical and Engineering Sciences*, *373*(2053), 20140372. https://doi.org/10.1098/rsta.2014.0372

Crawford, G. B., Admire, A. R., & Dengler, L. A. (2017). Spectral analysis of water level and velocity data from Crescent City Harbor during the April 1, 2014 Chilean tsunami. *Pure and Applied Geophysics*, *174*(8), 2987–3002. https://doi.org/10.1007/s00024-017-1616-9

Crawford, G. B., Admire, A., & Uslu, B. (2026). Predictability of tsunami currents from water levels in Humboldt Bay: Evidence of a strongly damped basin response [Preprint]. *ESS Open Archive*. https://doi.org/10.22541/essoar.15008785/v1

Crawford, G. B., Dolcetti, G., Admire, A., & Uslu, B. (2026). Data and Code for: Estimating Tsunami Currents in a Resonant Harbor Using Video-Based Analysis: Application to

Crescent City, California. *[Data set and software]*. *Zenodo*. https://doi.org/10.5281/zenodo.22131854

Dean, R. G., & Dalrymple, R. A. (1991). *Water wave mechanics for engineers and scientists* (Vol. 2). World Scientific Publishing Company.

Dolcetti, G., Hortobágyi, B., Perks, M., Tait, S. J., & Dervilis, N. (2022). Using noncontact measurement of water surface dynamics to estimate river discharge. *Water Resources Research*, *58*(9), e2022WR032829. https://doi.org/10.1029/2022WR032829

Elipot, S., Hughes, C., Olhede, S., & Toole, J. (2013). Coherence of western boundary pressure at the RAPID WAVE array: Boundary wave adjustments or deep western boundary current advection? *Journal of Physical Oceanography*, *43*(4), 744–765. https://doi.org/10.1175/JPO-D-12-067.1

Fritz, H. M., Borrero, J. C., Synolakis, C. E., & Yoo, J. (2006). 2004 Indian Ocean tsunami flow velocity measurements from survivor videos. *Geophysical Research Letters*, *33*(24), L24605. https://doi.org/10.1029/2006GL026784

Fritz, H. M., Phillips, D. A., Okayasu, A., Shimozono, T., Liu, H., Mohammed, F., Skanavis, V., Synolakis, C. E., & Takahashi, T. (2012). The 2011 Japan tsunami current velocity measurements from survivor videos at Kesennuma Bay. *Geophysical Research Letters*, *39*(7), L00H28. https://doi.org/10.1029/2011GL050686

Kalligeris, N., Skanavis, V., Tavakkol, S., Ayca, A., El Safty, H., Lynett, P., & Synolakis, C. (2016). Lagrangian flow measurements and observations of the 2015 Chilean tsunami in

Ventura, CA. *Geophysical Research Letters*, *43*(10), 5217–5224. https://doi.org/10.1002/2016GL068796

Lamb, H. (1932). *Hydrodynamics* (6th ed.). Cambridge University Press.

Lynett, P. J., Borrero, J. C., Weiss, R., Son, S., Greer, D., & Renteria, W. (2012). Observations and modeling of tsunami-induced currents in harbors and ports. *Geophysical Research Letters*, *327-328*, 68-74. https://doi.org/10.1016/j.epsl.2012.02.002

Lynett, P. J., Borrero, J., Son, S., Wilson, R., & Miller, K. (2014). Assessment of the tsunami-induced current hazard. *Geophysical Research Letters*, *41*(6), 2048–2055. https://doi.org/10.1002/2013GL058680

Muraro, F., Dolcetti, G., Nichols, A., Tait, S. J., & Horoshenkov, K. V. (2021). Free-surface behaviour of shallow turbulent flows. *Journal of Hydraulic Research*, *59*(1), 1–20. https://doi.org/10.1080/00221686.2020.1870007

NOAA Center for Operational Oceanographic Products and Services. (2025). *1-minute water level data for Crescent City, CA (Station 9414806)* [Data set]. National Oceanic and Atmospheric Administration. https://api.tidesandcurrents.noaa.gov/api/prod/

Rabinovich, A. B. (2009). Seiches and harbor oscillations. In Y. C. Kim (Ed.), *Handbook of coastal and ocean engineering* (pp. 193–236). World Scientific Publishing. https://doi.org/10.1142/9789812819307_0009

The MathWorks Inc. (2025). *MATLAB and MATLAB Copilot* (Release R2025a) [Software]. The MathWorks Inc. https://www.mathworks.com

Wilson, B. W. (1972). Seiches. In V. T. Chow (Ed.), *Advances in Hydroscience* (Vol. 8, pp. 1–94). Academic Press.

Wilson, R. I., Admire, A. R., Borrero, J. C., Dengler, L. A., Legg, M. R., Lynett, P., McCrink, T. P., Miller, K. M., Ritchie, A., Sterling, K., & Whitmore, P. M. (2013). Observations and impacts from the 2010 Chilean and 2011 Japanese tsunamis in California (USA). *Pure and Applied Geophysics*, 170(6–8), 1127–1147. https://doi.org/10.1007/s00024-012-0527-z

Winsemius, H. C., Dolcetti, G., & Peña-Haro, S. (2026). *IWaVE - Image Wave Velocimetry Estimation* (Version v0.4.0) [Software]. Zenodo. https://doi.org/10.5281/zenodo.21299642

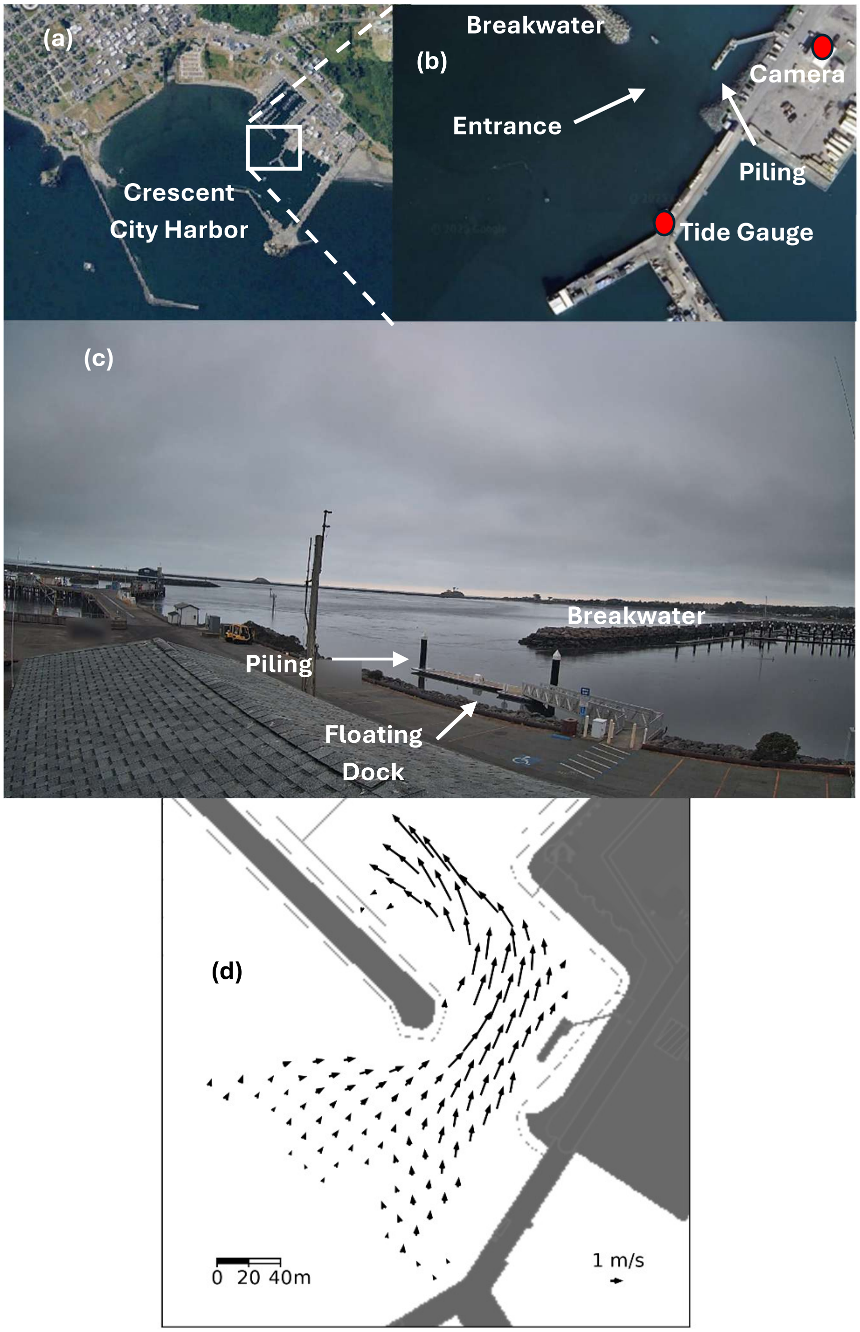

Figure 1. Study location, security camera view, and representative surface velocity field in Crescent City Harbor, California. (a) Regional map of Crescent City Harbor, California (base map: USGS). (b) Satellite image of study site, showing small boat basin entrance, NOAA tide gauge (Station 9414806), and security camera (imagery: © Google Earth, Airbus, SIO, NOAA, U.S. Navy, NGA, GEBCO). (c) Representative raw security camera frame. (d) Ortho-rectified 1-min average surface velocity field derived from IWaVE during a peak flood phase (09:08–09:09 PDT on July 30, 2025).

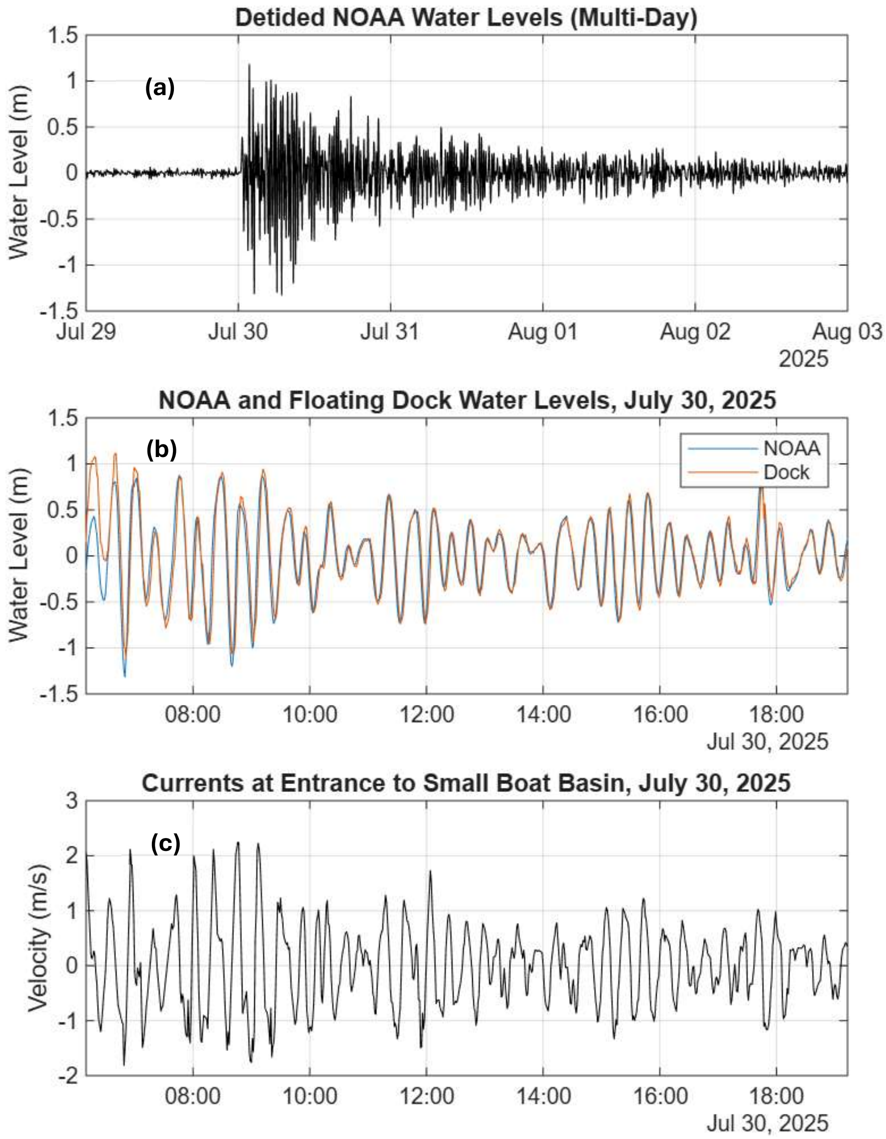

Figure 2. Water level and entrance current velocity time series during the July 30, 2025 Kamchatka tsunami at Crescent City Harbor. (a) Detided 1-minute sea surface elevation from the NOAA tide gauge at Citizens Dock spanning July 29 to August 3, 2025. The initial tsunami arrival occurred at ~00:24 PDT on July 30 (maximum amplitude 1.10 m at 01:45 PDT). (b) Comparison between detided NOAA tide gauge water levels (blue) and optically tracked floating dock elevations (orange) during daylight observation hours on July 30 (06:10–19:13 PDT). (c) Detided primary-axis surface velocity time series extracted at the small boat basin entrance channel (positive flood into basin, negative ebb out of basin).

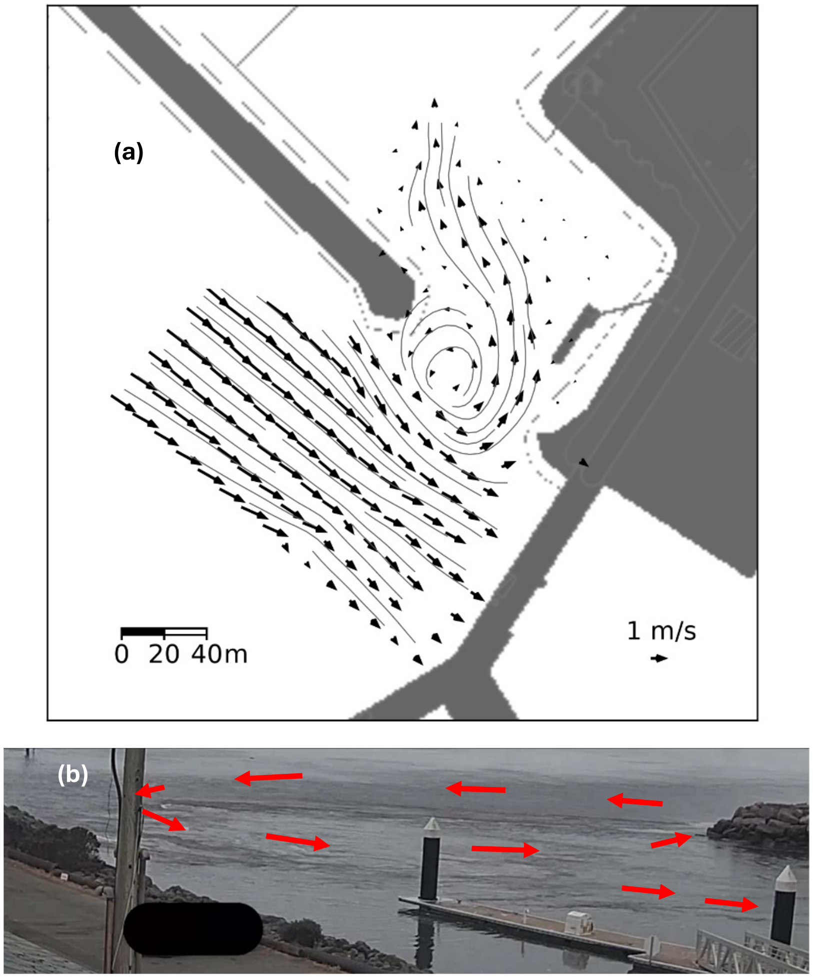

Figure 3. Observation of a transient eddy at the small boat basin entrance. (a) One-minute average surface velocity vector field and overlaid streamlines at 06:19–06:20 PDT on July 30, 2025, demonstrating counter-clockwise shear-driven vortex formation at the entrance. (b) Cropped raw security camera frame at 06:19:37 PDT, visually confirming the surface feature in the raw footage. Arrows denote the direction of fluid motion.

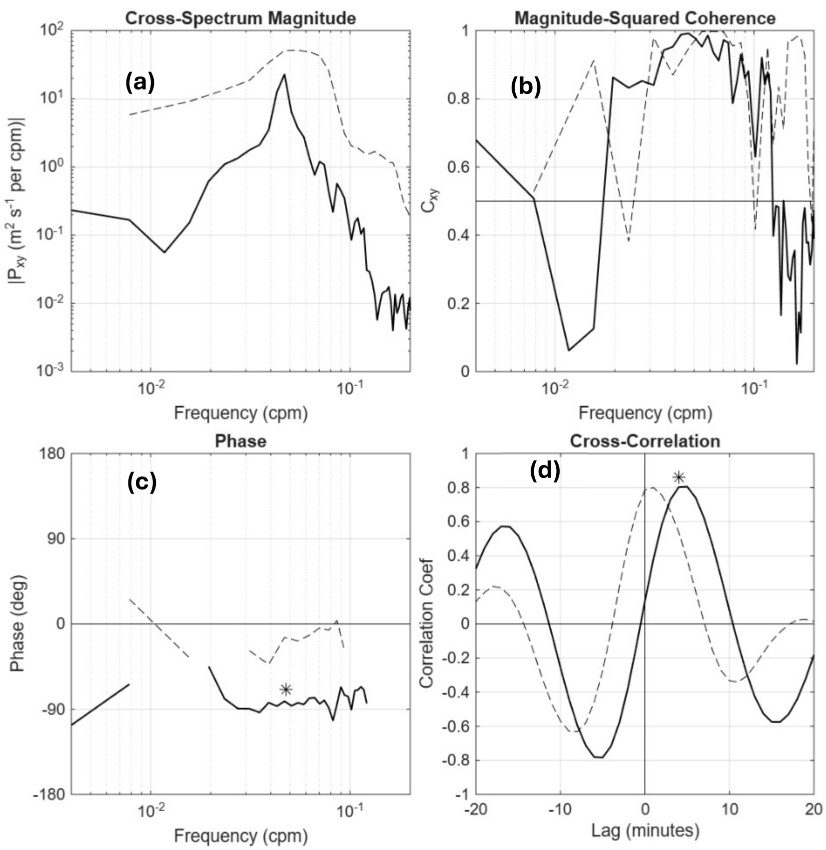

Fig. 4. Cross-spectral and cross-correlation relationships between water level elevation and current velocity at the small boat basin entrance. (a) Cross-power spectral density magnitude; (b) squared spectral coherence (C2); (c) spectral phase difference (negative values indicate velocity leads elevation); (d) normalized cross-correlation. Solid lines represent 2025 Kamchatka tsunami observations (floating dock water levels vs. entrance currents); dashed lines represent 2011 Tohoku tsunami observations (NOAA tide gauge water levels vs. entrance currents). Asterisks in (c) and (d) mark corresponding MOST numerical model predictions at the dominant 0.047 cpm (21 min) resonant peak (phase lag: –66°; peak correlation lag: +3.5 min; see also Fig. S3).